APPENDICES

Appendix 1

Modeling Files of LabVIEW Programming

Single View of The Linear Back-Projection (LBP) Algorithm:

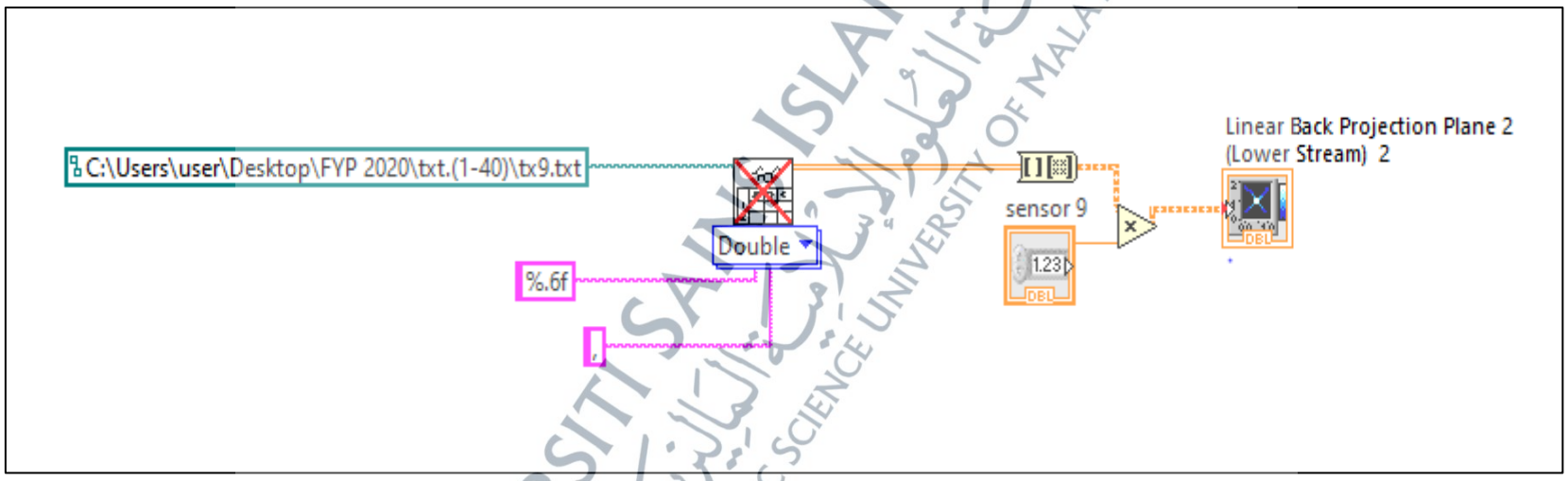

LabVIEW Graphical Coding for View 1 To 6 In The 1st Projection:

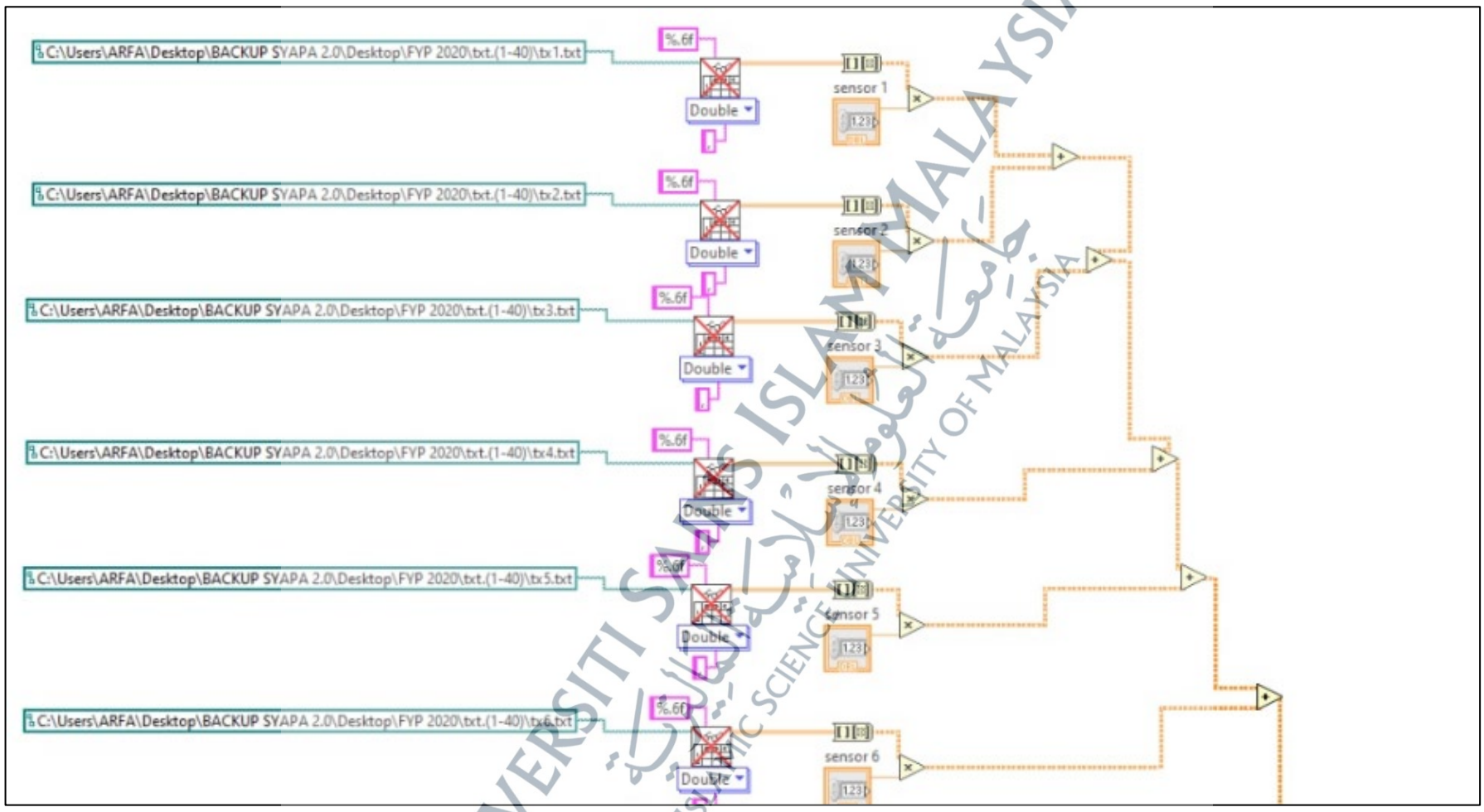

LabVIEW Graphical Coding for View 35 To 40 In The 1st Projection:

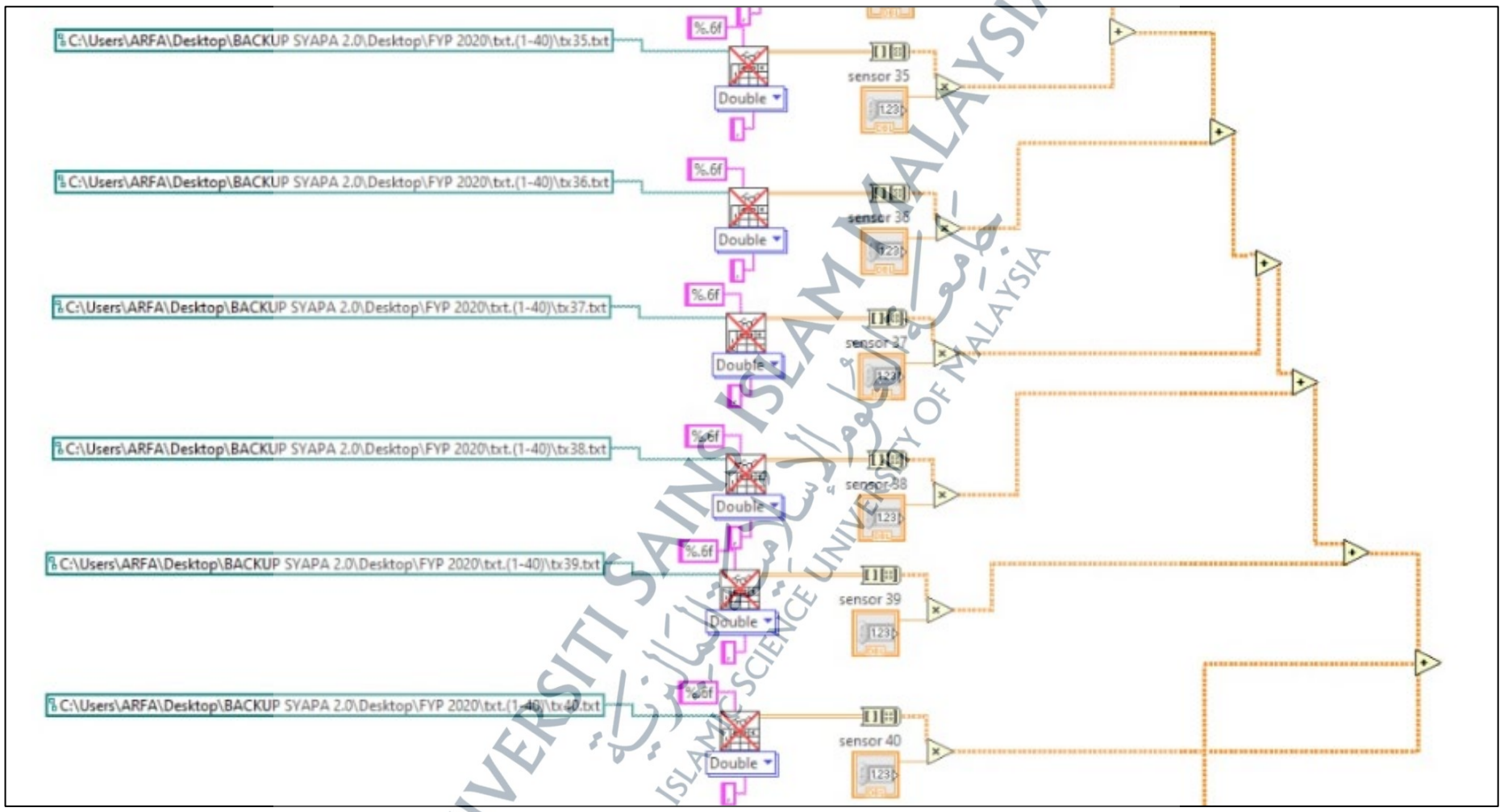

LabVIEW Graphical Coding for Views 157 To 160 In The 4th Projection:

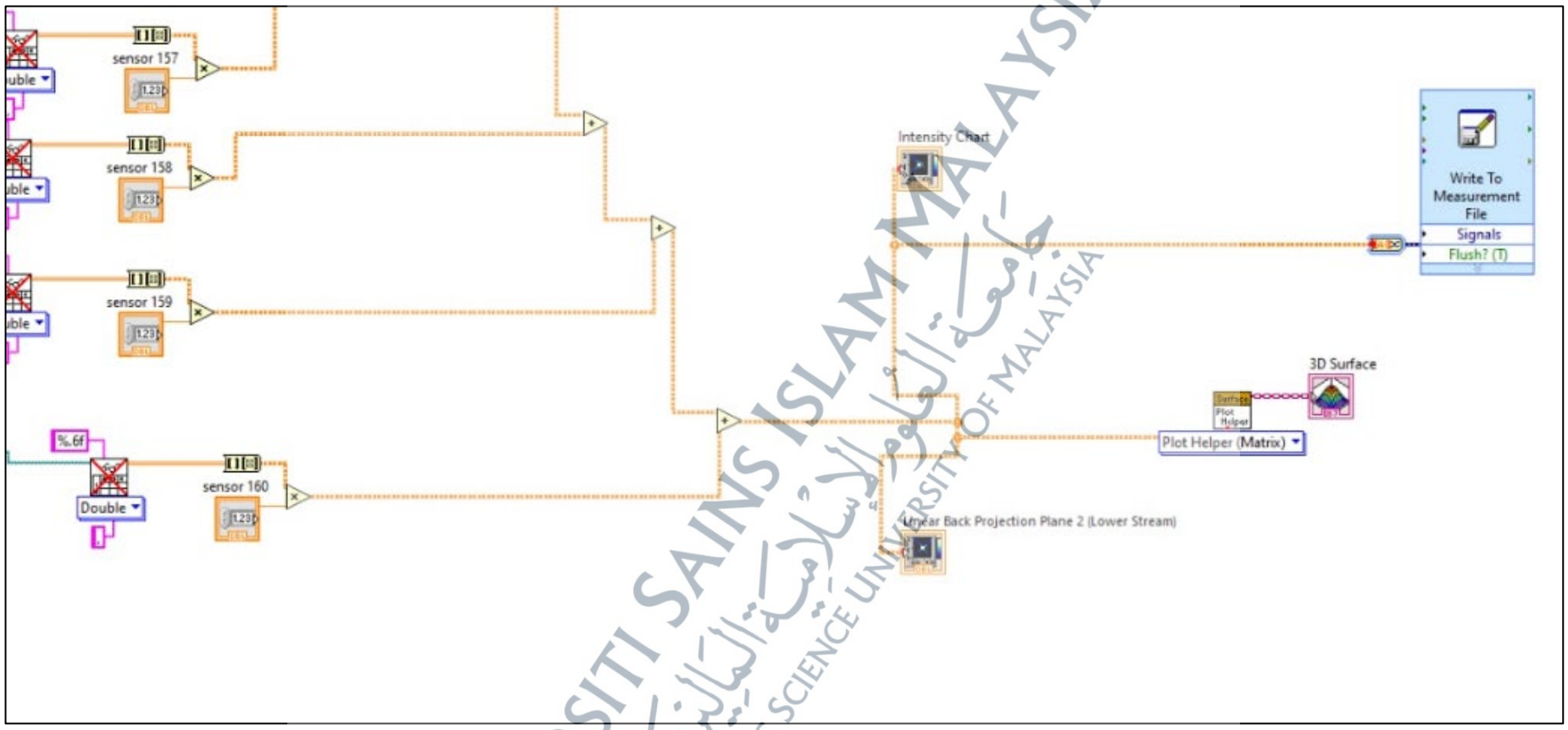

Appendix 2

National Journal

1. **Syarfa Najihah Raisin**, Juliza Jamaludin and Fatinah Mohd Rahalim. "A Ruby Stone Grading Inspection Using an Optical Tomography System." IOP Publishing Book Chapter, Artificial Intelligence and Spectroscopic Techniques for Gemology Applications, Chapter 4, Page 4-14 (2022)
2. **Syarfa Najihah Raisin**, Juliza Jamaludin, Irneza Ismail, Sharma Rao Balakrishnan, Bushra Naeem, Farah Aina Jamal Mohamad, Ahmad Syahmi Mohd Zain, and Abdullah Solihin Mohd Fauzi. "A Study of Object Transparency Via Charge-Coupled Device Mathematical Modelling Assessment." *Malaysian Journal of Science Health & Technology* 7 (2020).
3. **Syarfa Najihah Raisin,** Juliza Jamaludin, Irneza Ismail, Yasmin Abdul Wahab, Ruzairi Abdul Rahim, Mus'ab Sahrim, Sharma Rao Balakrishnan et al. "Simulation Study on CCD Tomography System for Ruby Stone Optical Properties." *Journal of Tomography System & Sensors Application Vol* 4, no. 1 (2021).
4. **Syarfa Najihah Raisin,** Juliza Jamaludin, Irneza Ismail, Yasmin Abdul Wahab, Ruzairi Abdul Rahim, Mus'ab Sahrim, Sharma Rao Balakrishnan et al. "Tomography System Towards the Industrial Revolution 4.0." *Journal of Tomography System & Sensors Application Vol* 4, no. 2 (2021).
5. Mohamad, Farah Aina Jamal, Ruzairi Abdul Rahim, Nasarudin Ahmad, Juliza Jamaludin, Sallehuddin Ibrahim, Mohd Hafiz Fazalul Rahiman, Nur Arina Hazwani Samsun Zaini, **Syarfa Najihah Raisin,** Navintiran, and Fatinah Mohd. "NDT-Defect Detection on Concrete using Ultrasonic: A Review." *Journal of Tomography System & Sensors Application Vol* 4, no. 1 (2021).

Conference

1. **Syarfa Najihah Raisin**, Juliza Jamaludin, Irneza Ismail, Sharma Rao Balakrishnan, Bushra Naeem, Farah Aina Jamal Mohamad, Ahmad Syahmi Mohd Zain, and Abdullah Solihin Mohd Fauzi. (2020, December 9). A Study of Object Transparency Via Charge-Coupled Device Mathematical Modelling Assessment (pp. 147-150). *Postgraduate Seminar Faculty of Science and Technology.*
2. **Syarfa Najihah Raisin,** Juliza Jamaludin, Irneza Ismail, Yasmin Abdul Wahab, Ruzairi Abdul Rahim, Mus'ab Sahrim, Sharma Rao Balakrishnan et al (2021, March 3). Simulation Study on CCD Tomography System for Ruby Stone Optical Properties. *4TH International Workshop on Computed Tomography & Imaging Technology.*

Appendix 3

MJoSHT
Malaysian Journal of Science, Health & Technology
[mjosht.usim.edu.my]

Article

A Study of Object Transparency Via Charge-Coupled Device Mathematical Modelling Assessment

Syarfa Najihah Raisin[1], Juliza Jamaludin*[1], Wan Zakiah Wan Ismail[1], Irneza Ismail[1], Sharma Rao Balakrishnan[1], Mus'ab Sahrim[1], Bushra Naeem[2], Farah Aina Jamal Mohamad[1], Ahmad Syahmi Mohd Zain[1], Abdullah Solihin Mohd Fauzi[1]

[1]*Electronic Engineering Programme, Faculty of Engineering and Built Environment, Universiti Sains Islam Malaysia (USIM), 71800 Negeri Sembilan Malaysia.*
**Email: juliza@usim.edu.my*

[2] *Balochistan University of Information Technology, Engineering and Management Sciences, Jinnah Town, Samungli Road, Quetta, Pakistan.*
Email: bushra.naeem@buitms.edu.pk

Abstract— **This research discusses an application of Couple-Charge Device (CCD) linear sensor and laser diode in an optical tomography (OPT) system. Tomography is a system that could capture a cross-sectional image based on sensor data scattered across the periphery of the examining device in the non-invasive and non-intrusive framework. This project focuses on quantifying the level of object transparency based on CCD and mathematical modelling assessment. The objective of this project is to investigate the light refraction, reflection and absorption effect on object transparency. The study will include a discussion on the light parameters and its mathematical expression. The voltage output measured by CCD defines the degree of intensity of light obtained after penetrating through different object transparency. In conclusion, this research has successfully proved the potential of CCD in OPT configuration to detect different size diameters of a targeted transparent object, which is an air bubble in non-flowing crystal-clear liquid.**

Keywords— **Charge-Coupled Device (CCD); optical tomography; object transparency; LabVIEW programming.**

I. INTRODUCTION

Charge-Coupled Device (CCD) is an integrated light-sensitive circuit that stores and displays information. In order to prevent any serious damage that may occur in a system, the monitoring process of steam bubbling production is essential for the engineers. The percentage of gas in the fluid solution, the flow rate of gas, the presence and absence of gaseous liquids, the shape and diameters of gases are important details for process controls. CCD is used as the mechanism tool to deal with this issue together with the tomography process. Tomography is a tool for capturing a cross-sectional image based on sensor data scattered around the visualization system's periphery [1]. In detail, optical tomography is one of the non-invasive and non-intrusive tomography approaches. It is a non-hazardous tomography system to monitor multiphase flow processes [2].

The primary goal of this analysis is to examine the level of object transparency based on CCD through mathematical modelling evaluation. To achieve this goal, one important objective will be conducted – to generate the mathematical modelling from the investigation of light in the optical tomography system, which includes the investigation of the light refraction, reflection and absorption effect on object transparency. The voltage output measured by CCD represents the level of light intensity received after penetrating through different objects. As a result, this research proves the capability of CCD to detect the different size of object transparency that will eventually result in different values of output voltage.

II. LITERATURE REVIEW

CCD is a sensor that is sensitive to light intensity. It will convert the light intensity into voltage signals. This study involves three types of light characteristics; light absorption, reflection, and scattering. By going through a particular type of medium, light is attenuated. In the optical path, the density of an object gave attenuation exponentially to the output of the light based on Beer-Lambert Law shown in equations (1) and (2).

$$I_{out} = I_{in} e^{-\propto x} \quad (1)$$

$$\ln\left(\frac{I_{in}}{I_{out}}\right) = \propto x \quad (2)$$

From equation 2, α is the linear attenuation vector, and x is the distance traversed by the beam of light. From the ray sum of the coefficients of linear attenuation distributed along the path inside the target, the real logarithm of the intensity-to-transmit intensity factor incident is obtained. The losses of energy arise as light travels in the form of light reflectance across an interface. Reflectance, defined by the

symbol R and shown in equation (3), is the ratio of light reflected on each surface.

$$R = \left[\frac{n_1 - n_i}{n_1 + n_i}\right]^2 \quad (3)$$

Where n_1 is a transmitted refractive index and n_i is an incidence refractive index.

Below are the equations that are involved when light penetrated from air to Perspex (equation (4)) and from water to glass surfaces (equation (5)).

For air-perspex interface:

$$R = \left[\frac{1.5-1}{1.5+1}\right]^2 = 0.04 \; or \; 4\% \quad (4)$$

For water-glass interface:

$$R = \left[\frac{1.5-1.33}{1.5+1.33}\right]^2 = 0.0036 \; or \; 0.36\% \quad (5)$$

The R value is the minimum surface reflection and occurs on plane surfaces where the surface is normal to the light ray. This represents a greater fraction of ray reflection as the incident ray angle of incidence increases. The amount of light that the particle transmits is decreased by these reflective effects [3]. Based on Hecht E, the diffraction phenomena occurred when an opaque object located between a screen and a light source produces a bright and dark shadowy area. In Figure 1, the diffraction effect is known as Fresnel or Near-field diffraction due to the position – either the panel or the light source is near to the blockage or obstruction. Besides, there was Fraunhofer or Far-field diffraction whenever the source of light or the panel is distant from the blockage.

In a case where the particle or the targeted object is near to the linear CCD sensor (the length between the object and the sensor is 71 mm), the diffraction effect in the optical tomography method is expected to be primarily Fresnel diffraction. The diffraction effect is closely connected to the obstruction 's height. The effects of diffraction will be minimal if the particle size or obstruction is very high relative to the light source wavelength x. The diffraction effects become more prominent as the obstruction size decreased.

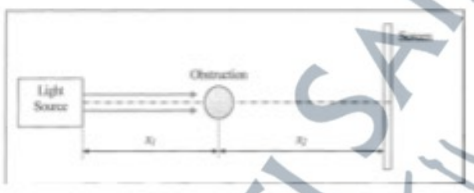

Figure 1. A light strikes an obstruction [4]

Each object has a degree of transparency in this universe. Based on its opacity, the transparency of the material will determine the capacity of light to pass through it. The intensity of light is mainly attributed to the CCD output voltage [4]. Once the beam is distorted by a compact object, the subsequent fringe pattern on the picture shows the diffraction effect, as shown in Figure 2 to Figure 4. Figure 4 shows that there are some light 'softens' at the edge of the shadow, even though a compact or opaque object acts as the barrier [4].

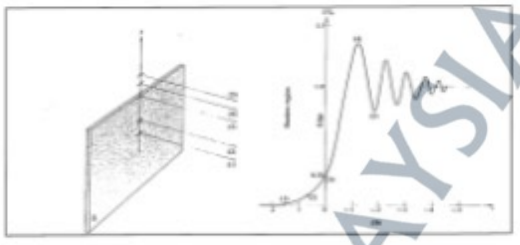

Figure 2. The opaque screen and the intensity distribution

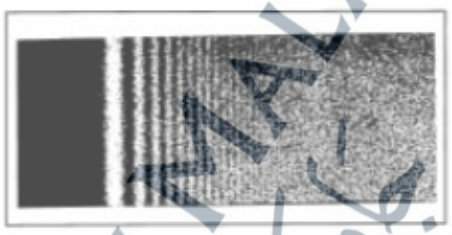

Figure 3. The fringe patterns

Figure 4. The shadow pattern cast by a Vs-inch diameter rod

The term transparency in optics is the property of letting light pass through something. It is a translucent material if some light can be seen through an object, but some details of the image are lost. Frosted glass, paper and some types of amber are examples of translucent materials. The word optical clarity is the ability to allow light to pass through something. This position-sensitive detector will assess where the sensor is struck by light [5]. In essence, imaging capture systems consist of an optoelectronic sensor and a device that converts digital code to an analogue form of signal. As a spatially uniform array, the sensor is a matrix of modelled small cells. The cell is a light-sensitive microscopic device that can generate electrical impulses pertaining to light incidents of different intensities. This sensor is sensitive to the light intensity but not to the colours, despite its photosensitivity. It is crucial to implement the optical filters to differentiate the three main colours, which are the red, green and blue in a selected pixel sensor. Instinctively, as in the human vision, three spectral bands (red, green, and blue) formalize the scene.

CCD sensor (Figure 5) has high affectability and exactness, high signal rates, a wide unique range and uses low power consumption. The basic principle of CCD is to measure the light ray dimension acquired by its sensors that are created using semiconductor components. Thus, CCD is

accepted to have the option to distinguish hazy items as it were. This is on the basis that the light that reaches their surface may imitate or absorb hazy posts. The existence and location of the object will be determined by the last measure of light power obtained by the CCD. These developments demonstrate that CCD has a high affectability to distinguish dull spots [6].

In different investigations, researchers explore the utilization of CCD linear sensors in an optical tomographic instrumentation framework implemented to estimate particles. Four CCD linear sensors are mounted around an octagonal flow pipe for a four-projection system. Optical tomography is commonly used both in manufacturing and medical industries [7]. There are several factors that make this form of tomography the best device for non-invasive and non-intrusive sensors. It is resistant to electrical interference and noise and consists of hard field sensors with high resolution. In estimating an object, the fundamental concept of the optical tomography system depends on its source of waves and radiation.

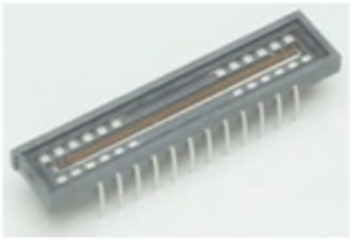

Figure 5. CCD Linear Array Sensor

The OPT system's primary idea is to observe the radiation force and wave generated within the midst of the intersection of the deliberate material. Additionally, the OPT system works to break down the structure and formation of objects. In fact, optical tomography sensors are recognized as opto-electronic sensors. There are three sections that constitute the basic construction of an optical tomography application: equipment (hardware), the application for collecting information (DAQ system) and programming. The block diagram of an optical diagram is shown in Figure 6 [8].

Figure 6: A block diagram of the optical tomography system

III. METHODOLOGY

Figure 7 illustrated the light travel and passed through three distinct instruments, which are the air, perspex and water. It can be observed that two modes of mathematical expression are involved in this simulation. There are;

a. Light attenuation due to absorption.
b. Light reflectance

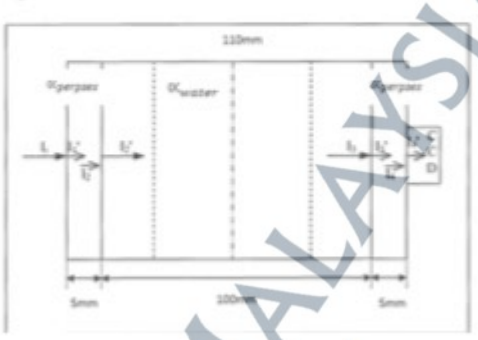

Figure 7. Side view of the overall measurement section

As light passes through different density of medium, the Beer-Lambert Law declared the amount of light strength or its intensity would be attenuated by multiplying it to the exponential attenuation as in equation 6. In equation 6, x represents the distance of light transverse. The alpha is a constant in this project that represents bubble air with a coefficient value of 1.0 and x is the manipulates value.

$$I_{out} = I_{in} e^{-\alpha x} \tag{6}$$

When light passes through the different medium or go through any object, the energy of photo (light) will be decreased, and thus, light reflectance occurred as in equation (7) and (8).

$$I_{Final\ reflection1} = I_{original} - \left[I_{initial} \left(\frac{n_2 - n_1}{n_2 + n_1} \right)^2 \right] \tag{7}$$

$$R = \left(\frac{n_2 - n_1}{n_2 + n_1} \right)^2 \tag{8}$$

Where R, n_1 *and* n_2 corresponds to reflection ration, transmitted refractive index and incidence refractive index respectively. In order to generate mathematical expression, both this light attenuation due to absorption and light reflectance are combined to calculate the transparency of the object via the CCD tomography method. Equation 9 to 27 shows the mathematical expression steps involved when there is an air bubble in the pipeline system full of water.

In this quantifying object transparency experiment, the study was further observed with the selection of air bubbles as the subject. The $n_{air\ bubble}$ which represents the air bubble's refractive index, was assumed to be [9]. Figure 8 is the modelled light striking the air bubble, which acts as the static object in the centre of the flow pipe. The diameter of the air bubble will be varied, which are 1mm, 3mm and 5mm.

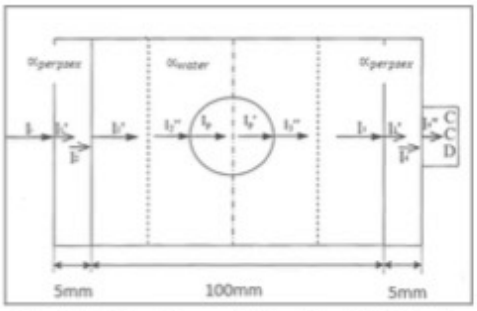

Figure 8. The light striking a static object in the middle of the pipe

Mathematical equation for calculating where there is an air bubble (1 mm)

Firstly, as the source of light entered the flow pipe, I_i (light intensity) is reduced due to the reflection at the air/perspex interface

$$I_1' = I_i - I_{reflection1} = I_i - \left[I_i\left(\frac{n_{perspex}-n_{air}}{n_{perspex}+n_{air}}\right)^2\right]$$

$$I_1' = I_i - \left[I_i\left(\frac{1.5-1}{1.5+1}\right)^2\right] = 0.96I_i \quad (9)$$

Light is then absorbed in travelling through perspex

$I_2 = I_1' e^{-(\alpha_{perspex} x 5mm)}$ where the $\alpha_{perspex}$ is $0.003mm^{-1}$ and the glass length, X = 5mm

$$I_2 = I_1' e^{-(0.003mm^{-1} x 5mm)} = 0.9851I_1' \quad (10)$$

Substitute equation 9 into 10 results into equation 11, which is

$$I_2 = 0.9851\,(0.96I_i)$$
$$I_2 = 0.9457I_i \quad (11)$$

I_2 is further reduced at the Perspex/water interface and becomes I_2';

$$I_2' = I_2 - I_{reflection2} = I_2 - \left[I_2\left(\frac{n_{water}-n_{perspex}}{n_{water}+n_{perspex}}\right)^2\right]$$

$$I_2' = I_2 - \left[I_2\left(\frac{1.33-1.5}{1.33+1.5}\right)^2\right] = 0.9964I_2 \quad (12)$$

Then, substitute equation 11 into 12 results into equation 13, which is;

$$I_2' = 0.9964\,(0.9457I_i)$$
$$I_2' = 0.9423I_i \quad (13)$$

The calculation below is the equation for the calculation of the light absorption in the length of the water, x of the 1 mm air bubble diameter measurement.

$$x = \frac{100mm - 1mm}{2} = 49.5mm, \quad (14)$$

I_2' transverse the cell being attenuated by water α = $0.00287mm^{-1}$

$I_2'' = I_2' e^{-(\alpha_{water} x 49.5mm)}$ where water length, X = 49.5mm

$$I_2'' = I_2' e^{-(0.00287mm^{-1} x 49.5mm)} = 0.8676I_2' \quad (14)$$

Substitute equation 13 into equation 14, hence it becomes equation 15;

$$I_2'' = 0.8175I_i \quad (15)$$

Next is the water-to-air bubble calculation (1 mm). I_p is the light intensity value due to the reflectance phase being conducted.

I_p is diminished due to the water-air bubble interface, therefore it becomes;

$$I_p = I_2'' - I_{reflection3} = I_2'' - \left[I_2''\left(\frac{n_{air\ bubble}-n_{water}}{n_{air\ bubble}+n_{water}}\right)^2\right]$$

$$I_p = I_2'' - \left[I_2''\left(\frac{1-1.33}{1+1.33}\right)^2\right] = 0.9799I_2'' \quad (16)$$

Replace equation 15 into equation 16. Hence, the parameter of I_2'' is replaced with $0.8175I_i$ and the value of I_p as in equation 17;

$$I_p = 0.8011I_i \quad (17)$$

Since the object of interest is an air bubble, no light absorption phenomena occurred within the next phase. Thus, the process continues due to the distortion of light reflectance in 1mm size of the air bubble. The calculation from the air bubble (1mm) to water. I_p' is the intensity value of light due to reflectance process.

$$I_p' = I_p - I_{reflection3} = I_p - \left[I_p\left(\frac{n_{water}-n_{air\ bubble}}{n_{water}+n_{air\ bubble}}\right)^2\right]$$

$$I_p' = I_p - \left[I_p\left(\frac{1.33-1}{1.33+1}\right)^2\right] = 0.9799I_p \quad (18)$$

Substitute equation 17 into 18, therefore equation 19 becomes;

$$I_p' = 0.7850I_i \quad (19)$$

I_p' is further attenuated by water length 49.5mm where $\alpha_{water} = 0.00287mm^{-1}$

$$I_3'' = I_p' e^{-(\alpha_{water} x 49.5mm)}$$

$$I_3'' = I_p' e^{-(0.00287mm^{-1} x 49.5mm)} = 0.8676I_p' \quad (20)$$

Substitute equation 19 into 20, hence it becomes;

$$I_3'' = 0.6811I_i \quad (21)$$

As light passes through from water to perspex, the intensity value of I_4' is the intensity value of light due to the reflectance process.

$$I_3 = I_3'' - I_{reflection4} = I_3'' - \left[I_3''\left(\frac{n_{perspex}-n_{water}}{n_{perspex}+n_{water}}\right)^2\right]$$

$$I_3 = I_3'' - \left[I_3''\left(\frac{1.5-1.3}{1.5+1.3}\right)^2\right] = 0.9949I_3'' \quad (22)$$

Substitute equation 21 into 22, then it becomes equation 23;

$$I_3 = 0.6776 I_i \quad (23)$$

As light crossing through the Perspex-glass phase, light absorption occurred.

$I_3' = I_3 e^{-(\alpha_{perspex} \times 5mm)}$ where the $\alpha_{perspex}$ is $0.003\,mm^{-1}$ and the glass length, X = 5mm

$$I_3' = I_3 e^{-(0.003\,mm^{-1} \times 5mm)} = 0.9851 I_3 \quad (24)$$

Substitute equation 23 into 24, therefore it becomes;

$$I_3' = 0.6675 I_i \quad (25)$$

As light passes through from water to Perspex, the intensity value of I_4 is the intensity value of light due to the reflectance process.

$$I_4 = I_3' - I_{reflection5} = I_3' - \left[I_3' \left(\frac{n_{air} - n_{perspex\ glass}}{n_{air} + n_{perspex\ glass}} \right)^2 \right]$$

$$I_4 = I_3' - \left[I_3' \left(\frac{1-1.5}{1+1.5} \right)^2 \right] = 0.96 I_3' \quad (26)$$

Replace equation 25 to equation 26, hence it becomes equation 27;

$$I_4 = 0.6408 I_i \quad (27)$$

As in equation 17, there is no light absorption in the air bubble, thus producing the final light intensity mathematical expression as in equation 27.

The procedure of equation 14 to 27 is repeated with 3mm and 5mm size of air bubble diameter.

IV. DISCUSSION

Table 1 below shows the result obtained from the theoretical mathematical calculation when there is an air bubble with a 1mm diameter, an air bubble with a 3mm diameter and a 5mm diameter. The output voltage of the CCD is theoretically determined using the formula:

$$Voltage_{CCD} = (1 - I_4') * 5 \quad (28)$$

From the CCD Sony ILX551A datasheet, the final light intensity equation is then multiplied to 5 based on the maximum voltage output of this optoelectronic sensor [10]. The relationship between the bubble size, the value of its final light intensity, and the calculated output voltage of the CCD is shown in the table below.

TABLE 1.
RELATIONSHIP OF BUBBLE SIZE AND VOLTAGE OF CCD

Diameter of air bubble (mm)	Distance of light transverse (mm)	Value of final light intensity I_4'	Voltage of CCD (V)
1	49.5	$0.6418 I_i$	1.79
3	48.5	$0.6453 I_i$	1.77
5	47.5	$0.6492 I_i$	1.75

Therefore, as the light intensity increases, the air bubble also increases in size. The graph below shows that the light intensity (air bubble size) is inversely proportional to the Linear Sensor of the Charge Coupled System (CCD). A decreasing value of the CCD voltage output is created by the increase in light intensity.

Figure 9. Graph plotted CCD voltage value versus the bubble size

IV. CONCLUSIONS

In this study, the relationship between the diameter of an air bubble, light intensity, and voltage of CCD is measured through mathematical expression identification. In conclusion, it is proven from the theoretical calculation that as the light intensity increases, the voltage of CCD also increases.

ACKNOWLEDGEMENT

The authors would like to thank to Universiti Sains Islam Malaysia and ADS research group for their cooperation in this research paper. The research is supported by the Fundamental Research Grant Scheme Ministry of Higher Education Malaysia (FRGS/1/2020/WAB07/USIM/02/1).

REFERENCES

[1] J. Abbaszadeh, H. A. Rahim, R. A. Rahim, and S. Samfi, "Frequency adjustment in ultrasonic tomography system with a metal pipe conveyor," *Sensors Mater.*, vol. 25, no. 6, pp. 379–387, 2013, doi: 10.18494/sam.2013.871.

[2] J. Jamaludin *et al.*, "A Review of the Optical Tomography

System," *J. Teknol.*, vol. 69, no. 8, pp. 1–6, Jul. 2014, doi: 10.11113/jt.v69.3287.

[3] M. Idroas, R. A. Rahim, R. G. Green, M. N. Ibrahim, and M. H. F. Rahiman, "Image reconstruction of a charge coupled device based optical tomographic instrumentation system for particle sizing," *Sensors (Switzerland)*, vol. 10, no. 10, pp. 9512–9528, Oct. 2010, doi: 10.3390/s101009512.

[4] M. idroas, "A charge coupled device based optical tomography instrumentation system for particle sizing," vol. PHD, 2004.

[5] D. Haires, "Optoelectronic Sensor - an overview | ScienceDirect Topics," 2013. https://www.sciencedirect.com/topics/engineering/optoelectronic-sensor (accessed Dec. 18, 2019).

[6] J. Jamaludin, R. A. Rahim, H. Binti, and A. Rahim, "Online Optical Tomography System Application of Charge-Coupled Device (CCD) for Object Detection in Crystal Clear Water," no. September 2018, 2016, doi: 10.31645/jisrc(2016).14.1.0006.

[7] J. Jamaludin *et al.*, "Jurnal Teknologi Full paper Introducing an Application of a Charged Coupled Device (CCD) in an Optical Tomography System," vol. 3, no. Ccd, pp. 97–102, 2015.

[8] J. Jamaludin, R. A. Rahim, M. Hafiz, F. Rahiman, and J. M. Rohani, "Analysis on the Effect of Sensor Views in Image Reconstruction Produced by Optical Tomography System Using Charge-Coupled Device," vol. 27, no. 4, pp. 1689–1696, 2018.

[9] J. Jamaludin, R. A. Rahim, H. A. Rahim, M. H. F. Rahiman, and J. M. Rohani, "Charge-Coupled Device based on optical tomography system for monitoring two-phase flow tomography system for monitoring," no. October, pp. 2016–2018, 2017, doi: 10.1049/el.2016.3084.

[10] "ILX551A datasheet(1/10 Pages) SONY | 2048-pixel CCD Linear Sensor (B/W)." https://html.alldatasheet.com/html-pdf/47512/SONY/ILX551A/81/1/ILX551A.html (accessed Jun. 24, 2020).

Appendix 4

TSSA Journal of Tomography System & Sensors Application Vol.4, Issue 1, March 2021
www.tssa.com.my e-ISSN: 636-9133

Simulation Study on CCD Tomography System for Ruby Stone Optical Properties

Syarfa Najihah Raisin[1], Juliza Jamaludin[1*], Imeza Ismail[1], Yasmin Abdul Wahab[2], Ruzairi Abdul Rahim[3], Mas' ab Sahrim[1], Sharma Rao Balakrishnan[1], Wan Zakiah Wan Ismail[1], Fatinah Mohd Rahalim[1], Farah Aina Mohd Jamal[3], Nurul Arina Hazwani Samsu Zaini [3]

[1*]Faculty of Engineering and Built Environment, Universiti Sains Islam Malaysia (USIM), 71800 Negeri Sembilan Malaysia.
[2]Faculty of Electrical & Electronics Engineering Technology, Universiti Malaysia Pahang, Pekan Campus, 26600 Pekan, Pahang, Malaysia.
[3]School of Electrical Engineering, Faculty of Engineering, Universiti Teknologi Malaysia, UTM Johor Bahru, 81310 Johor, Malaysia.

Corresponding author* email: juliza@usim.edu.my
Accepted 3 March 2021, available online 31 March 2021

ABSTRACT

Ninety percent of the ruby stones available worldwide come from Myanmar. Malaysia is known to be one of the countries that have been importing ruby stones for precious stone industries, manufacturing industries, medical and dentistry applications. There are several gemology tools which are used to investigate the grading of ruby stones such as loop, microscope, and dichroscope. Nevertheless, these tools are highly dependable on human visual assessment and require years of experience that may lead to error since ruby stone quality is evaluated based on its clarity and transparency. Hence, this paper addresses a simulation study on the optical properties of ruby stones via Charge-Coupled Device (CCD) Tomography approach. This paper indicates the capability of CCD and tomography system to analyze the ruby stone optical properties through image reconstruction based on the previous research. Linear Back Projection (LBP) algorithm will be used to construct two-dimensional image reconstruction of varieties ruby stones. From these image reconstructions, the transparency and blemishes of ruby stones can be analyzed.
Keywords: Ruby Stone, Object Transparency, Charged-Coupled Device (CCD), Tomography

1. Introduction

The optical property of ruby stone is beneficial for quantitative grading of this gemstone towards the gemologists, stones industries, manufacturing industries (drilling and cutting), medical and dentistry application. The grading valuation of ruby stone is categorized by its transparency and blemishes. There is a specific characterization of diamonds that influence their value and uniqueness. However, the impact of pricing differs. These characteristics are referred to 4Cs which are the carat weight, clarity, colour and cut [1]. The weight of a ruby is measured in carats. Five karats = 1 gram [2]. The higher the weight of the carat, the rarer the ruby thus the greater its value when all other conditions are equal from one variety towards another. Illustrated below is the approximate appearance of a well-cut oval-shaped ruby for the given carat weight.

Figure 1. The approximate appearance of a well-cut oval-shaped ruby for a given carat weight [2]

The substances trapped within the gem known as inclusions relatively indicate the clarity grading of the gemstone. A gemstone's clarity grade indicates the relative absence of inclusions (materials trapped inside the gem), cracks and blemishes (surface deficiencies) affecting its appearance and surface area. There are very different clarity criteria for opaque and translucent gems than for clear gems [3].

Colour has an important role in the diamond demonstration. For some consumers, it's a hard C to comprehend, but it is an important part of the entire value view that is required to make purchasing decisions. Ruby differs in colour depending largely on their chromium and iron content. Consequently, rubies have various prevalent colours from different parts of the world such as in Cambodia, India, Myanmar, Sri Lanka, Tanzania, Vietnam, India, Tajikistan and Pakistan. Rubies, mainly red, span from brownish and purple to orange and pinkish. The most commonly used method of colour grading is the one established by GIA [4]. It has 23 grades of letters that run from D (colourless) to Z (light yellow, brown, or grey).

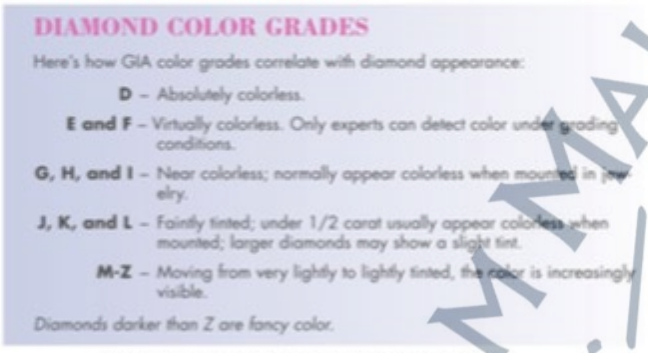

Figure 2. The diamond colour grade based on GIA [4].

Cutting is the most difficult aspect of the 4Cs [4] from a theoretical point of view. But it is also the top beauty attribute for the majority of diamonds. It has a huge influence on the appearance of a gem. Cut corresponds to the precision of the angles, ratios, proportion and shine of the ruby. It has a major effect on how light passes within the ruby and how it exits in the form of brilliance. There are five ways to classify the quality of gemstones based on their cut on the criteria of Clerk [5]; symmetry, magnification, contrast with similar stones, windows and cabochons. However, most gems are meant to have normal shapes. There are numerous gemology tools to investigate the ruby stone grading valuation. Available devices such as binocular microscope loupe [6] and portable dielectric tunable forensic lens [7] are used for ruby stone inspection. The basic principle of the system is magnifying the image of the ruby stone structure for visual inspection. Nevertheless, this is not a systematic and standardized technique to identify the grading of ruby stone transparency and blemishes. Therefore, this paper focuses on the optical properties of ruby stone via LabVIEW programming simulation through CCD and Tomography approaches.

2. Methodology

The main aim of this paper is to introduce a simulation study on CCD tomography system for ruby stone optical properties. Meanwhile, two objectives had been selected in order to gain the main aim of this research, that is to examine the light intensity of ruby stone based on theoretical value, which involves the light refraction and the absorption effect to the ruby stone. The next objective is to design conceptual modelling of CCD tomography approach using LabVIEW software. This could be done by establishing the octogen orientation concept for the CCD and ruby stone placement for conceptual modelling. The data used in this simulation is provided from the first objective.

2.1 Optical properties of Ruby Stone

From Figure 3 , it shows the light passes through two different mediums which are air and ruby stone. As light passes through different object medium, light attenuation will occur due to light absorption, light reflectance and light scattering. As the complex mathematical model, light scattering and the diffraction effect are neglected in this calculation with the additional fact that the wavelength of light incident used (laser light) is too small compared to the size of diameter of the interest object [7]. This can be concluded that there are two types of algorithms involved in this simulation, which is light attenuation due to;

1. Light absorption.
2. Light reflectance.

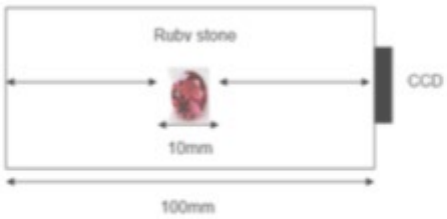

Figure 3. Light penetration through ruby stone and CCD.

2.1.1 Light absorption

Light is attenuated when it passes through from a medium to another medium, where attenuation phenomena happened due to absorption. All the three different mediums consist of respectively coefficient value α which will be used in the Beer-Lambert Law shown below.

$$I_{out} = I_{in}e^{-\alpha x} \tag{1}$$

From this formula, the output of light intensity is multiplied by the exponential attenuation of medium density when light passes through it. Whereby, x is the distance of light transverse.

2.1.2 Light reflectance

Energy of photo (light) will decrease when light goes through the different medium or passes through any object next to it. The light reflectance equation is

$$I_{Final\,reflection1} = I_{initial} - \left[I_{initial}\left(\frac{n_2 - n_1}{n_2 + n_1}\right)^2\right] \tag{2}$$

$$R = \left(\frac{n_2 - n_1}{n_2 + n_1}\right)^2 \tag{3}$$

R = Reflection ration
n_1 = Transmitted refractive index
n_2 = Incidence refractive index

Both of this light attenuation due to absorption and light reflectance are integrated to produce mathematical expression for this project.

2.2 Mathematical expression for a system consists of a laser, ruby stone and CCD.

Firstly, as a source of light entered the black box, I_i (light intensity) is reduced due to the reflection at the air/ruby stone interface.

$$I_1' = I_1 - I_{reflection1} = I_1 - \left[I_1\left(\frac{n_{rubystone} - n_{air}}{n_{rubystone} + n_{air}}\right)^2\right]$$

$$I_1' = I_1 - \left[I_1\left(\frac{1.762 - 1}{1.762 + 1}\right)^2\right] = 0.9238I_i \tag{4}$$

Light is then absorbed when travelling through a ruby stone.

$I_2 = I_1' e^{-(\alpha_{rubystone} x 10mm)}$ where the $\alpha_{rubystone}$ is $0.003mm^{-1}$ and the ruby stone length is assume, $X = 10mm$

$$I_2 = I_1' e^{-(0.003mm^{-1} x 10mm)} = 0.99I_1'$$

$$I_2 = 0.9238I_i \quad (5)$$

$$I_2' = I_2 - I_{reflection2} = I_2 - \left[I_2\left(\frac{n_{air} - n_{rubystone}}{n_{air} + n_{rubystone}}\right)^2\right]$$
$$I_2' = I_2 - \left[I_2\left(\frac{1-1.762}{1+1.762}\right)^2\right] = 0.9238I_2$$
$$I_2' = 0.8535I_i \quad (6)$$

I_2 is further reduced at the ruby stone/air interface.
The final light intensity ratio when a light strike through the ruby stone with $n_{ruby\ stone} =$ 1.762 and $\propto_{rubystone}$ is $0.003mm^{-1}$ is $\frac{I_2'}{I_i} = 0.8535$.

2.3 Image Reconstruction

Laboratory Virtual Instrument Engineering Workbench (LabVIEW) is National Instruments' system-design framework and visual programming language development environment [8]. LabVIEW is widely used on a range of operating systems (OSs), including Microsoft Windows, various versions of Unix, Linux, and macOS, for data collection, instrument control, and industrial automation. In this project, the image is produced based on the Linear Back Projection (LBP) algorithm. Figure 4 and 5 show the graphical coding for both light attenuation due to light absorption and light refraction respectively.

i. Light absorption equation and the LabVIEW modelling graphical code.

$$I_{out} = I_{in}e^{-ax}$$
$$I_4 = 0.6408I_i \quad (7)$$

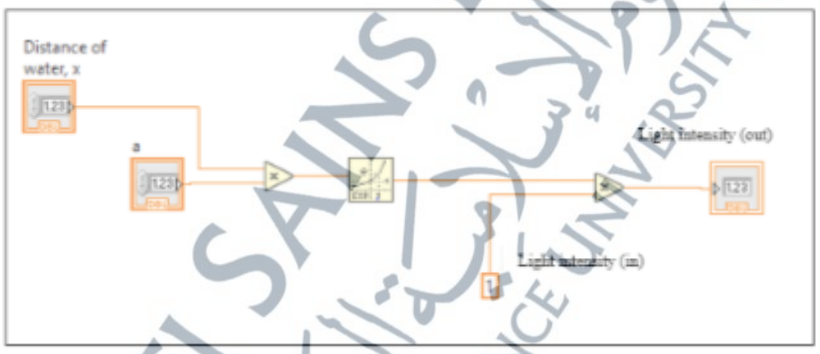

Figure 4. LabVIEW coding for light absorption calculation

ii. Light reflection equation and the LabVIEW modelling graphical code.

$$I_{Final\ reflection1} = I_{initial} - \left[I_{initial}\left(\frac{n_2 - n_1}{n_2 + n_1}\right)^2\right] \quad (8)$$

$$R = \left(\frac{n_2 - n_1}{n_2 + n_1}\right)^2 \quad (9)$$

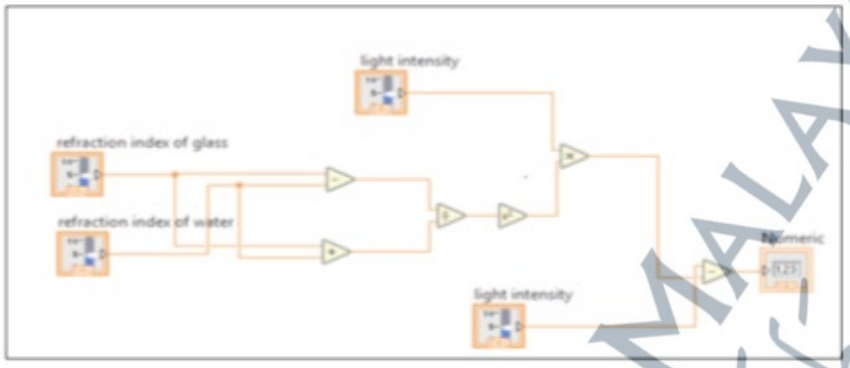

Figure 5. LabVIEW coding for light reflection calculation

This algorithm method is repeated for 160 times to get a clearer view as the number of pixels increases when the number of sensors used for the algorithm is increasing. The Equation (10) is shown below and the following figure shows the single linear projection view of the construction of 2D image [9].

$$V_{LBP\ (160\ views)}(x, y) = \sum_{tx=0}^{159} \sum_{rx=0}^{159} S_{tx,rx} x \bar{M}_{tx,rx} \quad (10)$$

Figure 6. Single view of linear back projection algorithm

3. Results

This research will apply the CCD tomography technique to investigate the transparency and blemishes of ruby stone. This is a non-invasive and non-intrusive technique which can determine the optical properties of an object accurately [10]. CCD, a light-sensitive integrated circuit that stores and displays the data of an image, will convert the light intensity received to the output voltage form. Research has been done by Jalaludin [11] [12] [13] on the optical tomography system using CCD. From these studies, CCD Sony ILX551A worked effectively with a low power laser diode, which is a red-light source. This CCD optical tomography system is capable to identify the existence of different object transparency and blemishes in crystal-clear water. The object transparency and blemishes classification are done by analyzing the light intensity received by CCD optical tomography after penetrating the object. Figure 7 shows the upper view of CCD optical tomography with the red-light source. The dark blue is the object which exists in the cylindrical pipeline full of crystal-clear water [11].

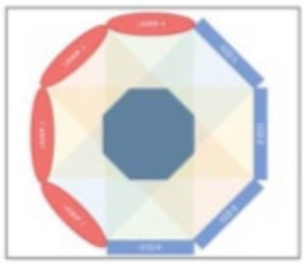

Figure 7. Upper view of CCD optical tomography with the red light source [11]

In 2020, S.N. Raisin [14] had constructed a simulation using LabVIEW programming to distinguish the image reconstruction detected by CCD in optical tomography method. This research will be the guideline for the expected output from different transparency and clarity of a ruby stone. Table 1 below shows the simulation for the image detected with different size of diameter, transparency and opacity [14].

Table 1. The comparison for the image detected with different transparency and opacity [14].

Transparent Object	Solid Object
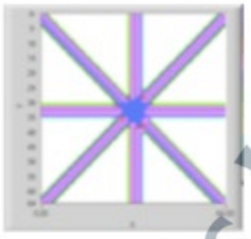 (a)	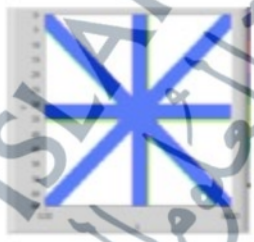 (b)
 (c)	 (d)

4. Discussions

The first simulation is done by assuming the size of (a) transparent object and the (b) solid object is 2mm. Table 1(a) and (b) showed sensors 20, 21, 22, 60, 61, 62, 100, 101, 102, 140, 141 and 142 are used to get the intercept modelling location of the transparent and solid object when the size of diameter is 2mm. The second simulation is done by assuming the size of (c) transparent object and the (d) solid object is 5mm. Table 1 (c) and (d) showed sensors 16, 17, 18, 19, 20, 21, 22, 56, 57, 58, 59, 60, 61, 62, 96, 97, 98, 99, 100, 101, 102, 136, 137, 138, 139, 140, 141 and 142 are used to get the intercept modelling location of the transparent and solid object when the size of diameter is 5mm [14].

5. Conclusion

In conclusion, this paper indicates the capability of CCD and tomography system to analyze the ruby stone optical properties through image reconstruction. To validate this hypothesis, two objectives were outlined and need to be achieved as well throughout this project simulation development. The first objective is to model the light characteristic equation based on the optical tomography system. The first objective is indeed a crucial point to gain. The proposed block diagram of ruby stone in the CCD tomography system consists of an arrangement of a different medium, which will attenuate the light incident from the laser beam before it reaches the CCD. The laser was the transmitter while the CCD was the receiver. The second objective is to construct the 2-D images that was proven by the previous research through the comparison of different level of object transparency. The images of captured data are reconstructed based on Linear Back Projection (LBP) Algorithm shows that the difference images formed as different level of object opacity placed in the measurement section.

Acknowledgement

The authors would like to thank to Universiti Sains Islam Malaysia and ADS research group for their cooperation in this research paper. The research is supported by the Fundamental Research Grant Scheme Ministry of Higher Education Malaysia (FRGS/1/2020/WAB07/USIM/02/1).

References

[1] D. Council, "Begining Jewelry sales," vol. 7, 2014.

[2] *Ruby Guide,* Italy: CIBJO, The World Jewellery Confideration, 2008.

[3] "What Do the GIA Gem Clarity Grading Codes Mean?," Gem Society, [Online]. Available: https://www.gemsociety.org/article/gia-gem-clarity-grading-codes. [Accessed 22 January 2021].

[4] "A Consumer's Guide to Gem Grading.," International Gem Society, [Online]. Available: https://www.gemsociety.org/article/a-consumers-guide-to-gem-grading. [Accessed 1 1 2021].

[5] S. Mukherjee, "Applied mineralogy: applications in industry and environment.," *Springer Science & Business Media,* 2012.

[6] Liao, Kai-Wei, K. J. Lu, R. C. Luo and J. A. Yeh., "Portable dielectric tunable forensic lens design for jadeite analysis.," *International Conference on Optical MEMS and Nanophotonics (OMN),* 2016.

[7] M. Idroas, "A charge coupled device based optical tomography instrumentation system for particle sizing," *Ph. D, Sheffield Hallam University,* 2004.

[8] T. Jeffrey and K. Jim, LabVIEW for Everyone: Graphical Programming Made Easy and Fun (3rd Edition), (National Instruments Virtual Instrumentation Series), vol. 79, 2006.

[9] J. Jamaludin and R. A. Rahim, "Online optical tomography system for detecting and measuring the diameters of solid and transparent objects.," *IEEE Sensors Journal,* vol. 16, no. 16, pp. 6175-6183, 2016.

[10] J. Jamaludin, M. Z. Zawahir, R. A. Rahim, F. R. M. Yunus, N. M. N. Ayob, S. R. A. Muhammad, N. S. Fadzil, Z. Zakaria and M. H. F. Rahiman, " A review of tomography system," *Jurnal Teknologi,* vol. 64, no. 5, pp. 47-51, 2013.

[11] J. Jamaludin, R. A. Rahim, M. H. F. Rahiman and J. M. Rohani, "Charge-coupled device based on optical tomography system for monitoring two-phase flow.," *Electronics Letters ,* vol. 53, no. 5, pp. 331-333, 2017.

[12] J. Jamaludin, R. A. Rahim, H. A. Rahim, M. H. F. Rahiman, S. Z. M. Muji and J. M. Rohani., " "Charge coupled device based on optical tomography system in detecting air bubbles in crystal clear water." Flow Measure," *Flow Measurement and Instrumentation,* vol. 50, pp. 13-25, 2016.

[13] J. Jamaludin, R. A. Rahim, H. A. Rahim, H. F. Rahiman, S. Z. M. Muji, N. S. M. Fadzil and L. P. Ling, "Introducing an Application of a Charged Coupled Device (CCD) in an Optical Tomography System.," *Jurnal Teknologi ,* vol. 73, no. 3, pp. 97-102, 2015.

[14] S. N. Raisin, LabVIEW Programming for the Investigation of Object Transparency Via Charge-Coupled Device Assessment, Undergraduate, Universiti Sains Islam Malaysia, 2020.

Appendix 5

TSSA Journal of Tomography System & Sensors Application Vol.4, Issue 2, Year 2021
www.tssa.com.my e-ISSN: 636-9133

Tomography System Towards the Industrial Revolution 4.0

Syarfa Najihah Raisin[1], Juliza Jamaludin[1*], Fatinah Mohd Rahalim[1], Fauzun Abdullah Asuhaimi[1], Wan Zakiah Wan Ismail[1], Irneza Ismail[1], Yasmin Abdul Wahab[2], Ruzairi Abdul Rahim[3], Farah Aina Mohd Jamal[3], Nurul Arina Hazwani Samsu Zaini [3]

[1*] Faculty of Engineering and Built Environment, Universiti Sains Islam Malaysia (USIM), 71800 Negeri Sembilan Malaysia.

[2]Faculty of Electrical & Electronics Engineering Technology, Universiti Malaysia Pahang, Pekan Campus, 26600 Pekan, Pahang, Malaysia.

[3] School of Electrical Engineering, Faculty of Engineering, Universiti Teknologi Malaysia, UTM Johor Bahru, 81310 Johor, Malaysia.

Corresponding author* email: juliza@usim.edu.my
Accepted 1 November 2021, available online December 2021

ABSTRACT

The world developed rapidly to provide better standard of living to the human being. Industrial revolution 4.0 promising in great revenue, investment and technological advancement to the society and various sectors. This paper presents an overview of tomography system towards the industrial revolution 4.0. Tomography is essentially a technique for showing an image representation through solid objects, such as a pipeline or the human body, in the two-dimensional and three-dimensional cross sections. Several tomography sensors, including optical tomography systems, ultrasonic tomography systems and an electrical tomography system, are discussed in terms of their hardware and image reconstruction. To provide a clear view of tomography system, a few examples of tomography system application in medical and process industries are discussed.

Keywords: tomography, image reconstruction, applications

1. Introduction

Industrial Revolution 4.0 or commonly known as Industry 4.0 has improve the manufacturing efficiency nowadays by investing in the new tools and technology. This has enhanced the human well-being and by revolutionizing the entire business operates and grows [1]. Since 1800s, manufacturing has evolved and still continue until today. The first industrial revolution occurred within the late 1700s to early 1800s [2]. The use of steam-powered engines is optimized by manually labor performed by peopled and sometimes assisted by animals. The introduction of electricity and the used of steel indicate the second phase of industrial revolution. This happened at the early of 20th century [3]. During this time, the assembly line concepts was introduced to produce mass production concept as a technique to increase the productivity. Eventually, electronic and computing technology began to emerge with manufacturing process starting in the late of 1950s [4].

The third industrial revolution started to shift the mechanical technology into the digitalized and automation framework [5]. The manufacturing experience automation, more complexation and sustainable production so that people could always efficiently and persistently operate the machine. The more comprehensively, interlinked and holistic approach was introduced in the past few decades as the Industry 4.0 take places. Those emerging of technology are emphasis to whole new level with the integration through the Internet of Things (IoT), cyberphysical systems (CPS), real-time data access, artificial intelligence (AI) and big data analysis. The

existing machine is then converted into self-aware and self-learning machines to boost their overall efficiency and maintenance management. This will eventually allow better cooperation between the physical and digital component, product and people across the place and time.

One of the rapid technologies developed in Industry 4.0 is the signal processing. Signal processing is one of the engineering approaches to model and interpret data representations received of physical events [6]. Such signals like images, sounds and other scientific measurement are required for data analyzing, synthesizing and modifying. This method has empowered the ability to communicate between the biotechnology and social interaction [6]. One of the examples of signal processing is the tomography system. Tomography system is commonly known for viewing the 2D or 3D images in a function of time. Figure 1 **Error! Reference source not found.** shows the basic block diagram for tomography system [7].

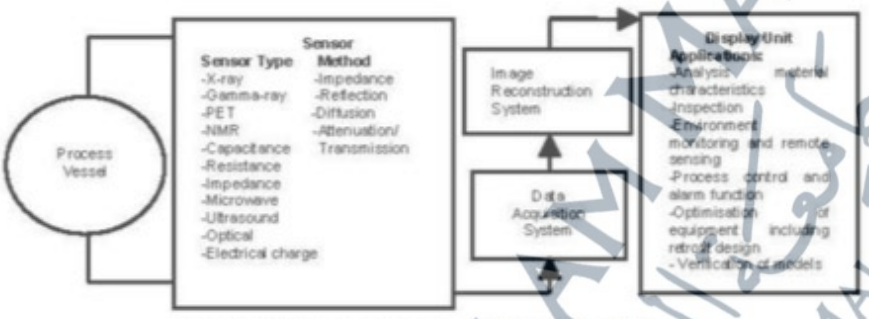

Figure 1. Block diagram of typical tomography system [7]

Huge application of tomography was applied in the medical industry since in 1950. For instance, the computed tomography (CT or CAT) is the composition of computer and X-rays to display pictures of the bones, other organs and body tissues [8]. Compared to a regular X-ray, this method shows more detailed in terms of the image constructed. Such as in industry, monitoring of the pipeline to avoid splitting of welding defects, cavitation degradation, media corrosion and material deterioration after a certain period of time may contribute to leakage and explosion accident [9]. Ultrasonic tomography was introduced to deal with this issue by giving high attenuation of ultrasonic energy to the steel pipes implementation. For multiphase flow industry, tomography system is the best approach for the application the requiring a non-intrusive and non-invasive monitoring systems [10].

2. Types of Tomography System

There are various types of tomography method has been existing more than 10 years ago such as ultrasonic tomography, capacitance tomography, optical tomography, impedance tomography, and resistance tomography. This tomography method also is developed because it is non- invasive and nonintrusive monitoring so that it significantly will help the new research to study and discover new knowledge about internal characteristics of matter such as to measure the velocity, diameter, distance, texture, mass flow rate, counter, shape and concentration [11]. Figure 2 shows the basic block diagram of a tomography system.

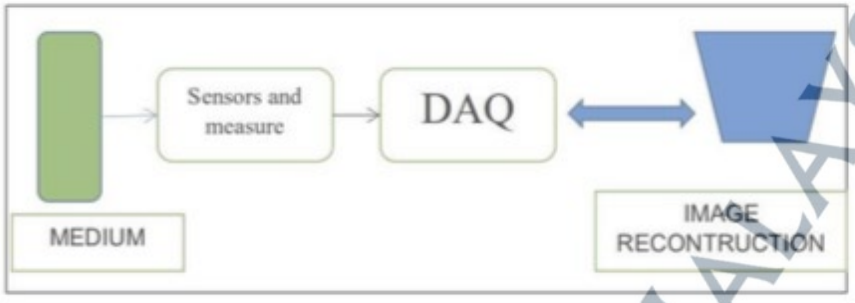

Figure 2. Basic block diagram of a tomography system [12]

Optical tomography approaches are non-intrusive in practice and secure since direct physical interaction with the flow is not required by the transducer. The system has high productivity and could increase production in the chemical industries. Optical techniques can produce high-resolution images for activities that treat transparent substances and other parts where the optical penetration is feasible. The optical tomography approach is competent to accomplish on-line measurements with its direct optical transmitter-receiver pairs [13].

Optical tomography reconstructs the image on the basis of optical radiation, sending a light beam from one edge and receiving light beam from another edge. By using various optical sensor types, such as lasers, linear CCDs, LEDs, etc., optical radiation can be produced. The drawback of optical tomography, however, refers to the restriction of its optical surface where it is not possible to put the sensors too close to each other in order to prevent reflection and to simple detect the image between the optical sensor areas [14].

As the sensing field is based on the calculation of the attenuation or absorption of light sources, the optical tomography device is called a hard-field sensor. Typically, the key principle of optical tomography is to analyze the structure and nature of objects by analyzing the strength of light after entering the target. Compared to other soft-field sensors, this optical tomography device has several benefits, which include being resistant to electrical noise or interference and also high resolution. Because of the speed of light, a tiny wavelength can have high resolution and insignificant response time as the speed of light is [15].

In tomography system, ultrasonic tomography (UT) has the potential for image reconstruction since it has the most effective sensing capability in differentiating the elasticity and the density of a certain object such as the liquid flows/bubble imaging. The ultrasonic sensor has massive advantages in tomography systems such as [16]. it is a non-invasive system where the sensor does not have direct contact to the fluid. It does not use any radioactive material which are safer compared to other type of tomography (positron emission tomography). In addition, it gives a quick response within a fraction of a second. Lastly, the transducers need only low energy levels to excite and this does not harm the plant or the materials being used. However, some of the limitation found in this acoustic characteristic is that, it can only effectively travel when there is a medium. Next in a multiphase flow application, high level of noise arise when the particle hit the flow pipe and thus researcher ought to take it into account during the analyzation process.

UT systems consist of the hardware and software parts [17] as shown in Figure 2. On one side of the pipe, the ultrasonic sensor transmitter that eventually connected to the amplifier circuit will convert the electrical energy signals into the ultrasonic waves. Then, the ultrasonic sensor receiver received the ultrasonic waves and transform it into the electrical signal. Figure 3 is the structure of the receiver part is consisting of the band pass, filters, lownoise amplifier and some cost data [18].

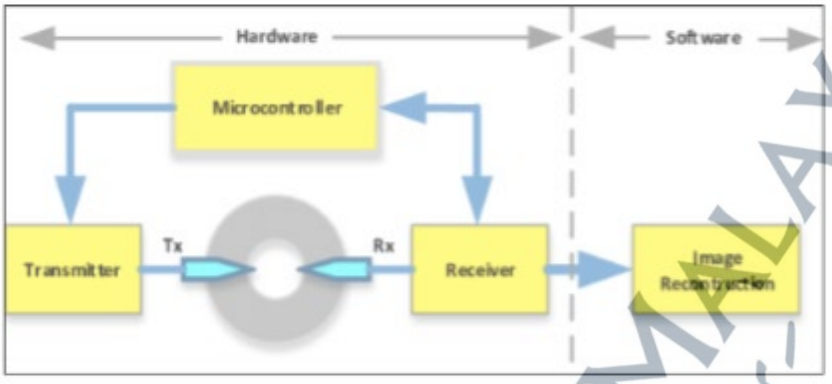

Figure 3. General block diagram of an ultrasonic tomography system [18]

The software part for image reconstruction in the ultrasonic tomography system is usually rely on the algorithm choose by the researches. The popular method used for the image reconstruction is the back-projection algorithm method. Initially, this method is introduced for use in X-ray tomography [16]. Back projection algorithm method provides low cost computational that eventually made it as the chosen method by the researchers. The back projection is solved once the solution for the forward problem obtained in this algorithm.

Liu et al [19] has addressed a circular scanning method used for imaging the location of breast cancer using the Piezoelectric Micromachined Ultrasonic Transducer (PMUT). The characteristic of breast cancer which has higher density eventually will distinguish the sound speed from the other elastic properties in the breast model [20]. Figure 4 below shows the location of masses that located in the centre of breast model for size 5.0 cm, 5.1 cm and 4.9 cm respectively.

Figure 4. Ultrasonic tomography of breast model using the ring system [19]

Electrical tomography has been used widely among the other type of tomography due to its advantages such as; low cost consumption, non-invasive capability non emitting radiation photon compared to some other type of tomography. There are a few types of electrical process tomography and some of the example are Electrical Resistance Tomography (ERT), Electrical Capacitance Tomography (ECT) and Electrical Impedance Tomography (EIT). In ERT process application, the EIT is the measurement of impedance that comprise of the imaginary part which are the reactance and the real part which referred to the resistance. The dominants properties in EIT are the real part. The ECT process sense the distribution of permittivity at non-conductive continuous process meanwhile the EIT implemented for a conductive continuous type of process. Basically, the Electrical Tomography system basically of electrode that function both as electrode and sensor. When current is injected into the electrode, subsequentially another side of electrode will measure the voltages value received. Until all the independent measurement completed to measure the voltage, the process is repetitive for the following electrode's couple. The difference in these three types of electrical tomography is the type of sensor used.

3. Application of Tomography System

Tomography have biggest contribution in medical field through its ability to obtain the information from human body that is valuable in clinical applications [21]. Tomography method such as X-ray, the Positron Emission Tomography (PET), optical coherence tomography (OCT) and Magnetic Resonance Imaging (MRI) are some of method used to visualize the tissue structure and detect the cancerous constituent in human body.

The widely used of tomography operation in medical sector is X-rays. In essentially, X-rays are kind of electromagnetic energy that is performed by particles known as photons [8]. The energy level of individual photons, also known as the wavelength of radiation, is the difference between X-rays and visible light rays. A clear detectable wavelength is susceptible to the human eye, but not to higher energy wavelengths that are shorter. As shown in Figure 5, an X-ray machine is consisting of a pair of electrodes in a glass vacuum composed of a cathode and an anode. A cathode is a heated filament. Heat sputters electrons off the surface of filaments.

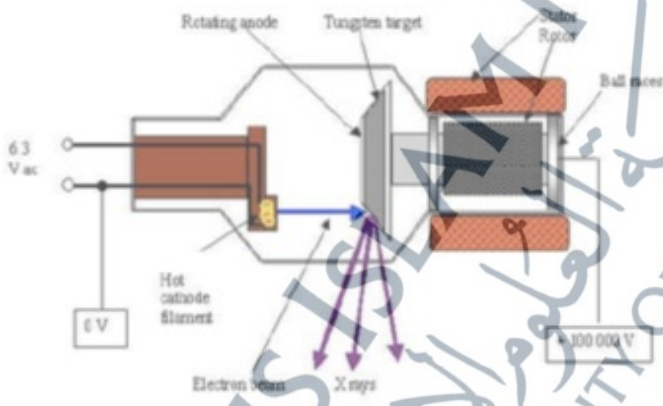

Figure 5.Building an X-ray glass vacuum tube [8]

To analyse blood vessels or other elements of the circulatory system the contrast medium will be infused into the patient's bloodstream. In combination with a fluoroscope, a contrast medium is also used. Whereas, a moving image of the X-ray is produced as the x-rays move through the body to a fluorescent screen in fluoroscopy. For the detection of the path of contrast media through the body, doctors can use fluoroscopy. Doctors may use the CT scanning to capture the moving X-ray images on film which combine processes in a digital form. The images are generated as a 2D model form and radiography [8] to display the information observed. Figure 6 shows the radiography X-ray picture of the chest, where the white image is shown showing the compact bone structure, the dark areas represent less dense structural elements that allow the passage of radiation.

Figure 6. A typical X-ray radiograph of the chest, in which the regions of bone are reflected in white [4]

The most prevalent disease in women worldwide is breast cancer. Thus, it is vital to have early detection approach on this issue. Liu et al. [19] address a modal to visualize the breast cancer imaging by using ultrasound computer tomography (USCT). The USCT method is radiation-free, painless and acceptable for all types of breasts compared to the mammography, the magnetic resonance imaging and hand-held ultrasound that result in dangerous radiation and painful compression to the examinee. Figure 7 and 8 below shows the experimental setup of this operation and the ultrasound tomography transducer acquisition setup respectively.

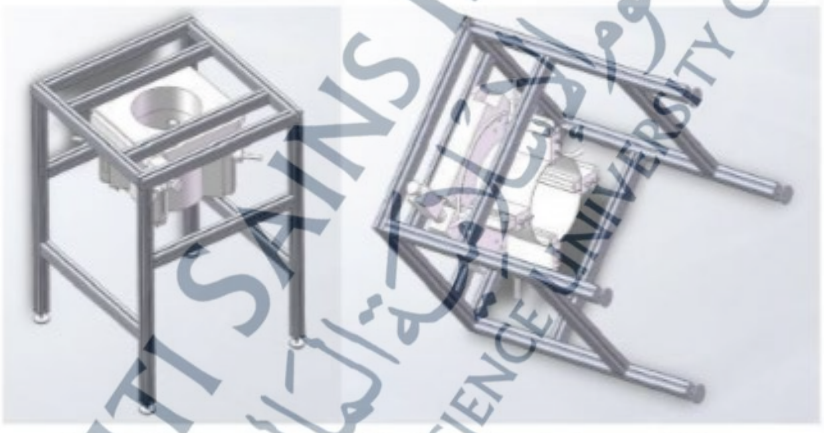

Figure 7. Experimental setup for the 3D ultrasound imaging ring system [19]

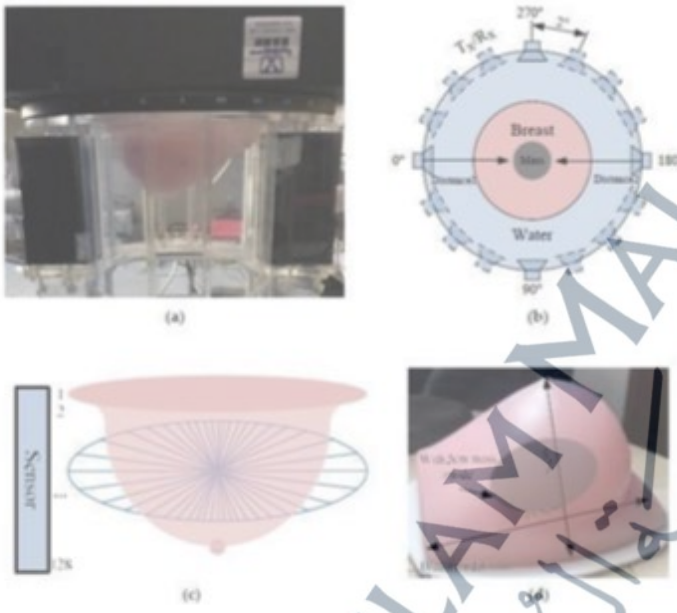

Figure 8. Ultrasound tomography transducer acquisition setup. (a) Placement of breast in the ring; (b) Transducer ring configuration platform; (c) Slice maps of ultrasound tomography imaging; (d) Breast Model [19]

Tomography system also widely used in process industries. For example, ultrasonic tomography is used in metal industries. After a certain period of time, cavitation erosion, media corrosion, welding defects cracking, substances leakage and explosion crashes might arise due to the degradation of materials [22]. In petrochemical industry, an issue potency results due to the defects and corrosion in pipeline and storage tank that will result in financial lost in terms of product losses, downtime in output, initiatives and fines for environmental cleanup [23]. Therefore, a monitoring operation ought to be implemented to reduce those risk that might harm to the human and environment. Tomography is one of the popular techniques used for monitoring process due to it low cost and simple circuit construction.

Hong et al [7] has review the application of various kind of sensor in tomography system for the metal industry. The steel pipes have worst internal reflections inside sealed pipes, besides its high ultrasonic energy attenuation and high bulk wave influence [7]. By using ultrasonic sensor, the ultrasound was examined by using two types of mode which are the longitudinal and shear waves. The ultrasonic wave attenuated due to a phenomenon such as scattering and diffusion in steel. The difference in velocity received by the ultrasonic sensor will then determine the different condition of material (crack, defect). The other method is by using the X-ray computed tomography (CT) to detect any crack and corrosion of steel pipe.

Ramsey et al. [24] inspect and control the quality of metal AM parts using this approach. The measurement includes the coordinate for dimensional metrology with inspecting the complex geometry and volume defects. Figures 9 and 10 below are the scans reveal the external and internal features of metal and the example of micro-CT technology in capturing the volume inside incandescent bulb, a fluorescent light bulb and an LED bulb respectively. Both picture proven better reconstruction of CT method to see the internal part of metal.

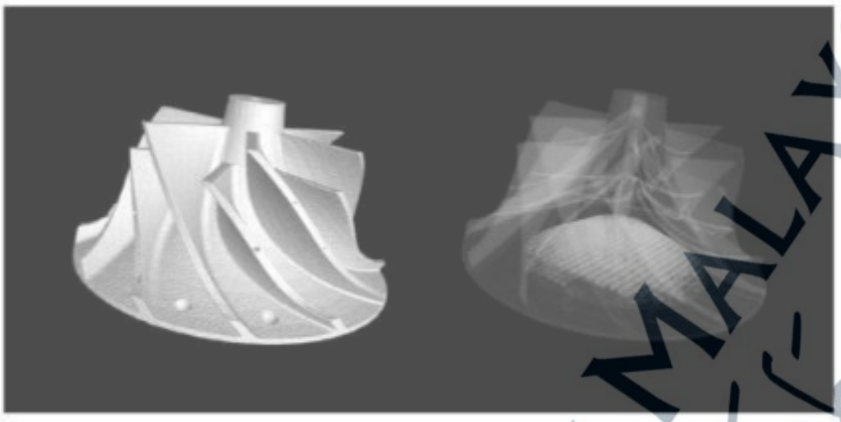

Figure 9. Scans can reveal external and internal features for checking [24]

Figure 10. CT image by Herminso Villarraga-Gómez demonstrating the capabilities of micro CT technology. From left to right: an Edison-style incandescent bulb, a fluorescent light bulb and an LED bulb [24]

Tomography has also provided massive contribution in powder industry. Dawning of a new era, the use of modern production skills in the adoption of new information technology plays a key role in economic competitiveness [25]. Industry revolution 4.0 encourages the convergence of smart systems for manufacturing and advanced information technology. In this recent age, additive manufacturing (AM) is regarded as an integral ingredient. It is important to implement non-conventional manufacturing method due to the need of mass customisation and manufacturing in Industry 4.0. Thus, because of its ability to build specialized objects with

sophisticated features (new materials, shapes), AM has become a leading technique for manufacturing customised goods.

Therefore, monitoring on the cross contamination of AM is required in order to utilize the manufacturing output efficiency. The laser powder bed fusion or known as L-PBF cross contamination Additive Manufacturing (AM) might change the chemical properties and shear stress in a component internally. It may also lead to fault formation and ultimately, reduce the mechanical efficiency of a part. Jamshidina et al. [26] implement an X-Ray Computed Tomography (CT) to monitor the in-process and cross contamination due to the tungsten powder particles in the consecutive layers. The 3D image reconstruction of the specimen that have been contaminated with the tungsten powder particle was illustrated in Figure 11 below where seventeen layers been detected contaminated with tungsten powder. Meanwhile, white stars labelled on the figure indicate the missing layer in the second layer from bottom. The image produced from figure below indicate that L4 and L6 have the minimum and maximum amount of powder deposited captured by the CT respectively [26].

Figure 11. The vertical cross-sectional views of the specimen contaminated by the tungsten [26]

Figure 12 shows the horizontal view of the distribution of tungsten powder in the six layers of contamination. A noticeable match was observed between the calibration images shown in Figure 38 and the actual distribution within the sample [26].

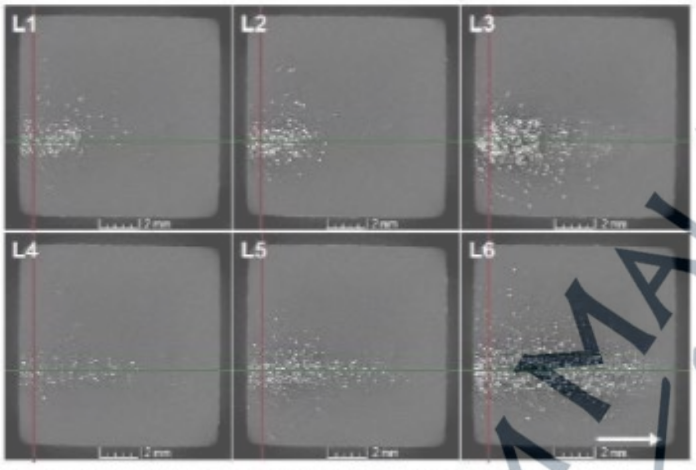

Figure 12. The horizontal cross-sectional views of the specimen contaminated with the [26]

In addition, Sinico et al. [27] study the characteristic of input material by using the cone-beam CT approach. Their work is to examines the ability and limitation of industrial microfocus CT (μ-CT) as one of the all-in-one method to describe the structure of metallic Additive Manufacturing (AM) powder, the variation of particle size and, possibly, the contamination of the feedstock powder. this work examines the ability and limits of industrial microfocus CT (μ-CT). This research strongly suggests the potential of μ-CT in detecting and eventually the degradation for cross-contamination of AM metal powder.

Apart from that Plessis et al. [28] identify a method for high resolution micro-CT scans and could provide detail analysis on the particular metal powder which is the Ti6A14V the common for laser powder bed fusion processes. This framework for image recognition gives data on internal (open or closed) porosity, particle size distribution (volume, field, sphericity) and the existence of contaminants such as higher density particles. The CT scan image below (Figure 13 and 14) shows clearly the pore space indicated in black circles and the 3D surface view of the exterior morphology of the particle.

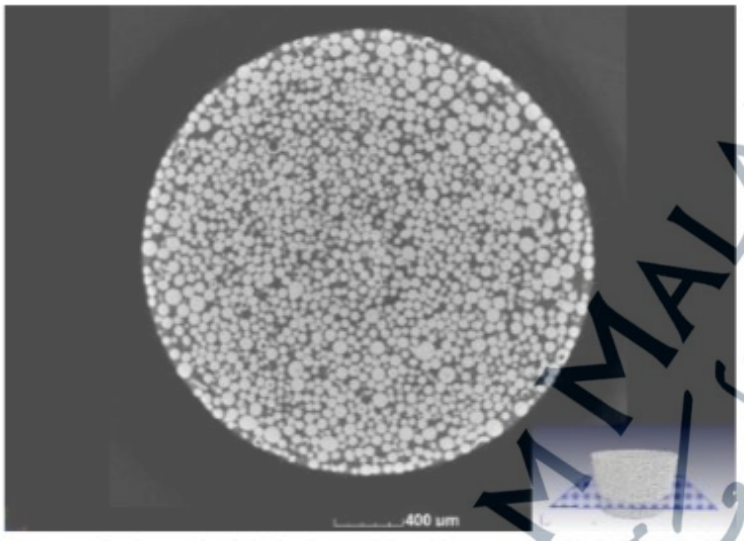

Figure 13. T slice image clearly indicating particles with pore spaces (blackcircles) [28]

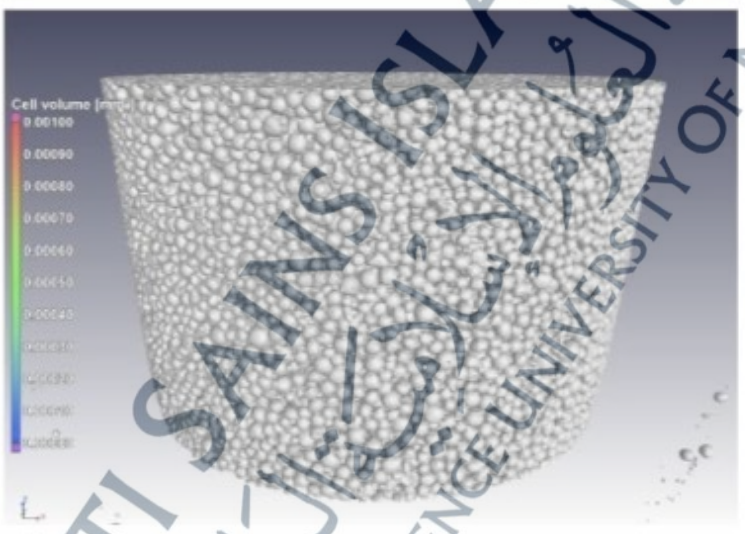

Figure 14. CT scan results showing 3D surface vie [28]

Next are the figures (Figure 15 and 16) for the 3D image of porosity analysis in terms of its size diameter and cross-sectional 2D image of particle size analysis respectively [28].

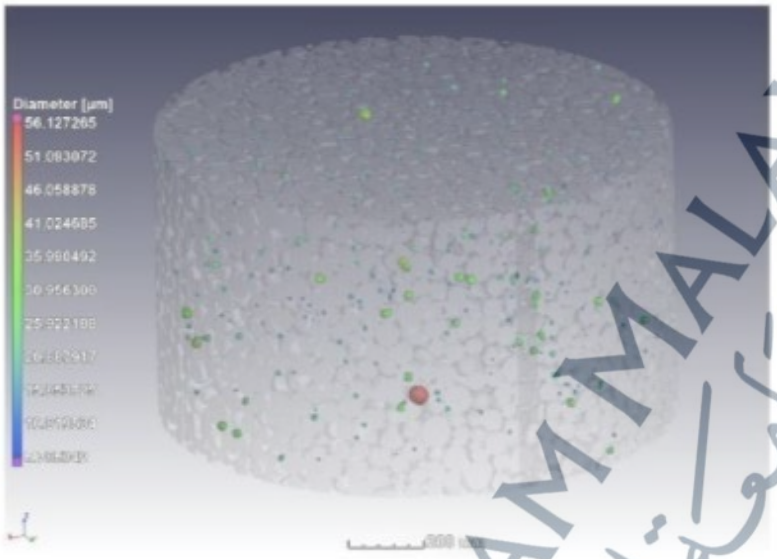

Figure 15. Porosity analysis of powders [28]

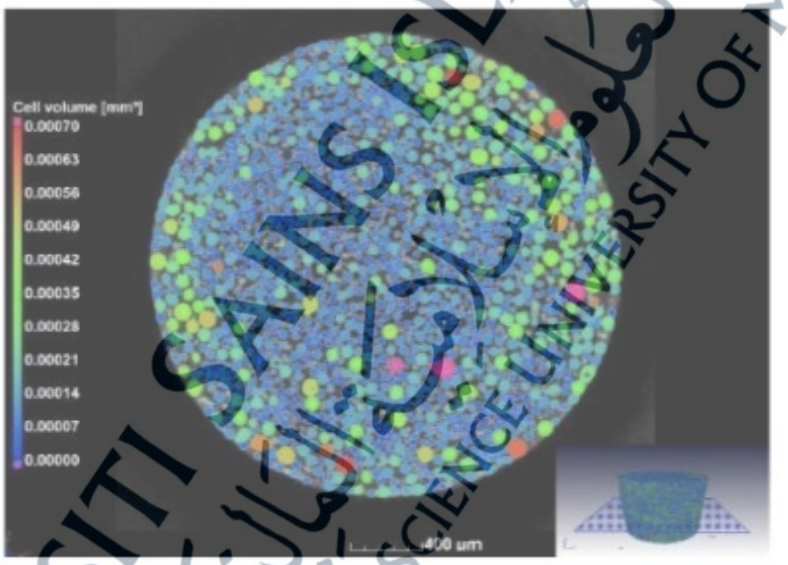

Figure 16. Particle size analysis - colour coding based on individual volume [28]

4. Conclusion

The concept and big picture of fourth industrial revolution allow efficient, smart, effective, development of individual and personalised production at the reasonable price. With the aid of smarter devices, smaller sensors,

cheap data processing and transmission enhance the communication from each other. This paper has highlighted the hardware and software framework on difference type of tomography system and its significant output to the mechanism efficiency. Tomography approach provide assembly analysis and reverse engineering technology where the feedback mechanism is dynamic and accurate. Tomography system has promising a better monitoring and analysing approach through image reconstruction and eventually contribute as an essential role in industrial revolution. The collection of data from production lines and optimisation of that data result into effective machine, energy saving and scheduling of optimised maintenance Furthermore, instead of its contribution in avoid false and losses in manufacturing, discussion on CSS pipeline monitoring also proved the capability of tomography to prevent harm to human life. In conclusion, this paper proven the ability and potential of tomography framework in the various sector of fourth industrial revolution.

Acknowledgment

The authors would like to thank Universiti Sains Islam Malaysia and ADS research group for their cooperation in this research paper.

References

[1] What is Industry 4.0? | The Industrial Internet of Things (IIoT) | Epicor MENA. (n.d.). https://www.epicor.com/en-ae/resource-center/articles/what-is-industry-4-0/ (accessed September 12, 2020).

[2] Industrial Revolution Definition, (n.d.). https://www.investopedia.com/terms/i/industrial-revolution.asp (accessed November 1, 2020).

[3] Industrial Revolution: Definitions, Causes & Inventions - HISTORY, (n.d.). https://www.history.com/topics/industrial-revolution/industrial-revolution (accessed November 1, 2020).

[4] What is Industry 4.0? | The Industrial Internet of Things (IIoT) | Epicor, (n.d.). https://www.epicor.com/en/resource-center/articles/what-is-industry-4-0/ (accessed November 1, 2020).

[5] J. Taalbi, Origins and pathways of innovation in the third industrial revolution 1, (n.d.). https://doi.org/10.1093/icc/dty053.

[6] Signal Processing 101 | IEEE Signal Processing Society, (n.d.). https://signalprocessingsociety.org/ourstory/signal-processing-101 (accessed September 12, 2020).

[7] L. En Hong, R.H. Abdul Rahim, Y. Md. Yunos, M.H. Izran Ishak, K.A. Danapalasingam, A.R. Wahab, M.H. Fazlul Rahiman, N.M. Nor Ayob, J. Pusppanathan, E.J. Mohamad, A review on the developments, potentials and challenges of application of metal products and in metal industry using process tomography system, J. Teknol. 73 (2015) 111–116. https://doi.org/10.11113/jt.v73.4429.

[8] N.A. Abd Rahman, L.E. Hong, R.H. Abdul Rahim, H. Abdul Rahim, N. Ahmad, S. Bunyamin, K.H. Abas, N.M. Nor Ayob, F.R. Mohd Yunos, M.S.B. Mansor, A review: Tomography systems in medical and industrial processes, J. Teknol. 73 (2015) 1–11. https://doi.org/10.11113/jt.v73.4398.

[9] J. Abbaszadeh, H.A. Rahim, R.A. Rahim, S. Sarafi, Frequency adjustment in ultrasonic tomography system with a metal pipe conveyor, Sensors Mater. 25 (2013) 379–387. https://doi.org/10.18494/sam.2013.871.

[10] W. Cailly, H. Walaszek, S. Brzuchacz, F. Zhang, P. Lasaygues, Pipe two-phase flow non-invasive imaging using Ultrasound Computed Tomography: A two-dimensional numerical and experimental

performance assessment, Flow Meas. Instrum. 74 (2020) 101784. https://doi.org/10.1016/j.flowmeasinst.2020.101784.

[11] C.N. Networks, K. Schabowicz, Detection of Flaws in Concrete Using Ultrasonic, (2020) 1–16.

[12] J. Jamaludin, M. K. Zawahir, R. A. Rahim, F. R. M. Yunus, N. M. N Ayob, S. R. A. Muhammad, N. S. Fadzil, Z. Zakaria, and M.H.F. Rahiman. "A review of tomography system." Jurnal Teknologi 64, no. 5 (2013)/ https://doi.org/10.11113/jt.v64.2131

[13] M. Idroas, R.A. Rahim, M.H.F. Rahiman, M.N. Ibrahim, Sensors and Actuators B : Chemical Optical tomography system based on charge-coupled device linear image sensors : Particle size measurement, Sensors Actuators B. Chem. 156 (2011) 572–577. https://doi.org/10.1016/j.snb.2011.02.001.

[14] Y. Abdul Wahab, R. Abdul Rahim, M.H. Fazalul Rahiman, S. Ridzuan Aw, F.R. Mohd Yunus, C.L. Goh, H. Abdul Rahim, L.P. Ling, Non-invasive process tomography in chemical mixtures - A review, Sensors Actuators, B Chem. 210 (2015) 602–617. https://doi.org/10.1016/j.snb.2014.12.103.

[15] J. Jamaludin, R.A. Rahim, H.A. Rahim, N.S.M. Fadzil, M.H.F. Rahiman, M.F. Jumaah, S.Z.M. Muji, and M.A.M. Yunus, 2014. A review of the optical tomography system. Jurnal Teknologi, 69(8)/ https://doi.org/10.11113/jt.v69.3287

[16] S. Ibrahim, M.A. Md Yunus, M.T. Md Khairi, M. Faramarzi, A review on ultrasonic process tomography system, J. Teknol. (2014) 1–5. https://doi.org/10.11113/jt.v70.3452.

[17] J. Abbaszadeh, H.A. Rahim, R.A. Rahim, Ultrasonic Tomography System : Optimizing the Frequency in a Metal Pipe Conveyor, 287 (2013) 572–576. https://doi.org/10.4028/www.scientific.net/AMM.284287.572.

[18] D. Ensminger, L.J. Bond, Ultrasonics: Fundamentals, technologies, and applications, third edition, 2011.

[19] C. Liu, C. Xue, B. Zhang, G. Zhang, C. He, The application of an ultrasound tomography algorithm in a novel ring 3D ultrasound imaging system, Sensors (Switzerland). 18 (2018). https://doi.org/10.3390/s18051332.

[20] E. Merc, Hybrid-array-based optoacoustic and ultrasound (OPUS) imaging of biological tissues, 203703 (2017). https://doi.org/10.1063/1.4983462.

[21] A. Haleem, M. Javaid, 3D scanning applications in medical field: A literature-based review, Clin. Epidemiol. Glob. Heal. 7 (2019) 199–210. https://doi.org/10.1016/j.cegh.2018.05.006.

[22] G. Shen, T. Li, Infrared thermography for high-temperature pressure pipe, Insight Non-Destructive Test. Cond. Monit. 49 (2007) 151–153. https://doi.org/10.1784/insi.2007.49.3.151.

[23] B.L.D. Oehl, Corrosion Testing with Real-Time 2-D Ultrasound Camera Imaging, Insp. J. (2014). https://inspectioneering.com/journal/2014-02-19/3788/corrosion-testing-with-real-ti (accessed September 29, 2020).

[24] A. Ramsey, H. Villarraga-Gómez, The inspection and quality control of metal AM parts with X-ray Computed Tomography (micro CT), Met. Addit. Manuf. 3 (2017) 1–7. https://www.researchgate.net/profile/Herminso_Villarraga-Gomez2/publication/318040879_The_inspection_and_quality_control_of_metal_AM_parts_with_Xray_Computed_Tomography_micro_CT/links/59565c9945851523ee91d997/The-inspection-andquality-control-of-metal-A.

[25] P. Zawadzki, K. Zywicki, Smart product design and production control for effective mass customization in the industry 4.0 concept, Manag. Prod. Eng. Rev. 7 (2016) 105–112. https://doi.org/10.1515/mper2016-0030.

[26] M. Jamshidinia, P. Boulware, J. Marchal, H. Mendoza, L. Cronley, S. Kelly, S. Newhouse, In-process monitoring of cross contamination in laser powder bed fusion (L-PBF) additive manufacturing (AM), Solid Free. Fabr. 2016 Proc. 27th Annu. Int. Solid Free. Fabr. Symp. - An Addit. Manuf. Conf. SFF 2016. (2016) 1366–1380.

[27] M. Sinico, E. Ametova, A. Witvrouw, W. Dewulf, Characterization of AM metal powder with an industrial microfocus CT: Potential and limitations, Proc. - 2018 ASPE Euspen Summer Top. Meet. Adv. Precis. Addit. Manuf. (2018) 286–291.

[28] A. du Plessis, P. Sperling, A. Beerlink, W.B. du Preez, S.G. le Roux, Standard method for microCT-based additive manufacturing quality control 4: Metal powder analysis, MethodsX. 5 (2018) 1336–1345. https://doi.org/10.1016/j.mex.2018.10.021.